NANO LETTERS

Letter

pubs.acs.org/NanoLett

Colossal Spin Transfer Torque Effect on Skyrmion along the Edge

Junichi Iwasaki,*[,†] Wataru Koshibae,[‡] and Naoto Nagaosa[†,‡]

[†]Department of Applied Physics, The University of Tokyo, 7-3-1, Hongo, Bunkyo-ku, Tokyo 113-8656, Japan

[‡]RIKEN Center for Emergent Matter Science (CEMS), Wako, Saitama 351-0198, Japan

Supporting Information

ABSTRACT: We study by the micromagnetic simulations the skyrmion motion along the edge driven by the current transverse to it. We found that (i) the velocity is enhanced by the factor of $\sim 1/\alpha$ (α: the Gilbert damping) with the maximum value determined only by the confining force from the edge, (ii) the inertia appear due to the confining potential with the coordinate perpendicular to the edge playing the role of the kinetic momentum, and (iii) the collision between the two skyrmions is almost elastic without causing any internal distortions.

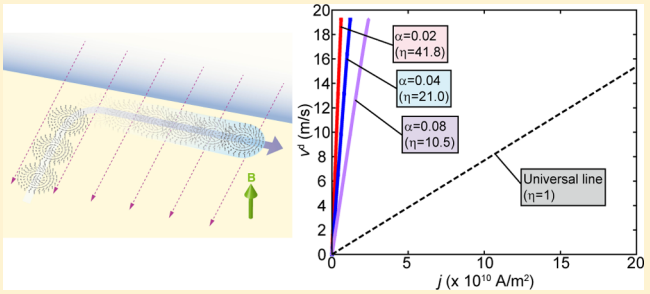

KEYWORDS: *Magnetic skyrmion, spintronics, micromagnetic simulation, magnetization dynamics*

Skyrmion,[1−9] a swirling spin texture recently found in chiral magnets with Dzyaloshinskii−Moriya (DM) interaction D under an external magnetic field B, is considered to be a promising candidate for the information carrier in magnetic memories and logic circuits. It is topologically stable as characterized by the skyrmion number Q, that is, an integer counting the number of times the spin direction wraps the unit sphere, and can be manipulated with ultralow energy consumption due to its extremely small threshold current density ($\sim 10^6$ A/m^2)[10−12] compared with that of the domain wall in ferromagnets ($\sim 10^{10}$−10^{12} A/m^2).[13−15] This can be understood within the framework of the Thiele equation[16] derived assuming the rigid body motion of the spin texture. Let $\mathbf{R} = (X, Y)$ be the center of mass coordinates, and the equation of motion reads[11,17]

$$\mathbf{G} \times (\mathbf{v}^s - \mathbf{v}^d) + \mathbf{D}(\beta \mathbf{v}^s - \alpha \mathbf{v}^d) + \mathbf{F} = 0 \qquad (1)$$

where $\mathbf{v}^d = \dot{\mathbf{R}}$ is the velocity of the spin texture, and $\mathbf{v}^s = -(pa^3/2eM)\mathbf{j}$ is the velocity of the conduction electrons, which can be identified as the current density $\mathbf{j}$ except a factor. Here, M is the magnetization, p is the spin polarization of the conduction electron, and a is the lattice constant. The third term $\mathbf{F}$ is the force acting on the spin texture from the boundaries, impurities, magnetic field, and so forth. The essential difference between the domain wall and the skyrmion is that the Magnus vector $\mathbf{G} = \mathbf{0}$ for the domain wall, whereas the $\mathbf{G} = \mathcal{G}\mathbf{e}_z$ with $\mathbf{e}_z$ being the unit vector along z direction and $\mathcal{G} = -4\pi$ for the skyrmion. The second term represents the dissipative force, where α is the Gilbert damping coefficient, β represents the nonadiabatic effect, and the components $\mathcal{D}_{ij}$ of the tensor $\mathbf{D}$ are $\mathcal{D}_{xx} = \mathcal{D}_{yy} = \mathcal{D} \sim 4\pi$ and 0 otherwise. Therefore, considering that $\alpha \sim \beta \sim 10^{-3}$−$10^{-2} \ll 1$, the dominant term is the first term for the skyrmion and, hence, $\mathbf{v}^d = \mathbf{v}^s$ immediately results when $|\mathcal{G}\mathbf{v}^s| \gg |\mathbf{F}|$ is satisfied. This relation indicates $|\mathbf{v}^d| \simeq 1$ m/sec for $j = 10^{10}$ A/m^2 for a reasonable set of parameters.[18] On the other hand, for the domain wall, the first term is missing and the dissipative second term becomes important to result in $\mathbf{v}^d = (\beta/\alpha)\mathbf{v}^s$ when $\beta|\mathbf{v}^s| \gg |\mathbf{F}|$ is satisfied. Here, note that the coefficient β in front of $|\mathbf{v}^s|$ leads to the large value of critical current density compared with the skyrmion. The advantage of the skyrmion over the domain wall is not clear at this stage because, in any case, the reasonably high speed operation requires large current density $j \sim 10^{10}$ A/m^2 to obtain $|\mathbf{v}^d| \sim 1$ m/sec in both cases.

The physical meaning of the Magnus vector $\mathbf{G}$ in eq 1 is that the X and Y coordinates of the skyrmion center are canonical conjugate to each other as in the case of a charged particle in two-dimensions under a magnetic field perpendicular to it (when mass is neglected). This analogy leads to the vital role of the edge on the dynamics of the skyrmions as in the edge channel of quantum Hall system, although the skyrmion motion is classical. Actually, it has been shown that the confining potential in the narrow constricted geometry completely changes the dynamics of a skyrmion.[19,20] Namely, the j−v^d characteristics changes from the universal one to that of the ferromagnetic domain wall, which is dependent on the ratio β/α and subject to the pinning effect when the current is along the edge.[19] Also, the emergence of the "mass" for the one-dimensional motion has been suggested, whereas the inertial motion has not been analyzed.[19] In particular, Sampaio et al.[20] demonstrated the relation $|\mathbf{v}^d| = \eta|\mathbf{v}^s|$ with large $\eta \sim 1/\alpha$ when the current is injected vertically to the plane. The similar situation is realized when one apply the in-plane current perpendicular to the edge.

Received: April 16, 2014
Revised: July 1, 2014
Published: July 2, 2014

In this paper, we investigate theoretically the dynamics of skyrmions near the edge of the sample under the influence of the confining potential by the numerical simulation of the Landau−Lifshitz−Gilbert (LLG) equation and an analysis by the Thiele equation. The focus is on the motion driven by the current transverse to the edge.

When the current is flowing in y direction across the edge along x direction between the chiral magnet and the lead, the skyrmion is trapped along the edge as shown in Figure 1. The

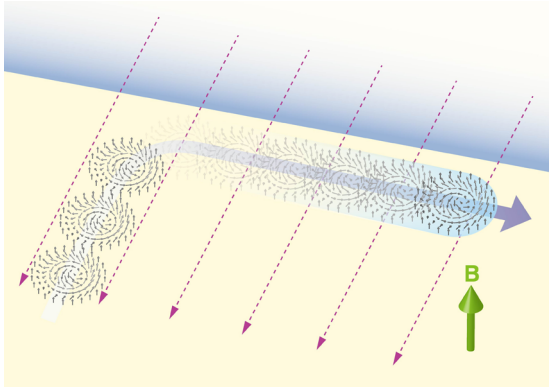

Figure 1. Schematic picture of skyrmion motion. In the free space, the skyrmion motion obeys the universal relation $v^{\mathrm{d}} = v^{\mathrm{s}}$, whereas its speed increases by a factor $\sim 1/\alpha$ when it is trapped along the edge and moves in the direction transverse to the current.

present situation can be described by setting $v_y^{\mathrm{d}} = v_x^{\mathrm{s}} = F_x = 0$ in eq 1. We explicitly write the two components of eq 1 as

$$\begin{cases} -\mathcal{G}v_y^{\mathrm{s}} - \mathcal{D}\alpha v_x^{\mathrm{d}} = 0, \\ -\mathcal{G}v_x^{\mathrm{d}} + \mathcal{D}\beta v_y^{\mathrm{s}} + F_y = 0 \end{cases} \tag{2}$$

From these equations, one can readily obtain

$$v_x^{\mathrm{d}} = -\frac{\mathcal{G}}{\mathcal{D}\alpha} v_y^{\mathrm{s}} \tag{3}$$

and

$$\left(\frac{\mathcal{G}^2}{\mathcal{D}\alpha} + \mathcal{D}\beta\right) v_y^{\mathrm{s}} = -F_y \tag{4}$$

Equation 3 means that η defined above is $\sim 1/\alpha$, which is of the order of 10^2−10^3 for the reasonable value of $\alpha \sim 10^{-3}$−10^{-2}.[20] Equation 4, on the other hand, determines the distance of the skyrmion from the interface. As shown in the Supporting Information of ref 19, the force F_y pushes back to the inside of magnet (repulsive force $F_y < 0$) when the distance from the interface is larger than ξ which is about the size of the skyrmion, while the skyrmion is attracted by the interface ($F_y > 0$) otherwise. The maximum repulsive force $F^{\max}$ determines the critical current density $(v_y^{\mathrm{s}})^{\mathrm{cr}}$, below which the skyrmion finds a steady position $Y = Y^*(v_y^{\mathrm{s}})$. However, it overcomes the potential barrier and disappears at the interface when $v_y^{\mathrm{s}} > (v_y^{\mathrm{s}})^{\mathrm{cr}}$. From eq 4, one obtains

$$(v_y^{\mathrm{s}})^{\mathrm{cr}} = \frac{F^{\max}}{\frac{\mathcal{G}^2}{\mathcal{D}\alpha} + \mathcal{D}\beta} \simeq \frac{F^{\max}\mathcal{D}\alpha}{\mathcal{G}^2} \tag{5}$$

and correspondingly, the maximum velocity of the skyrmion is given by

$$(v_x^{\mathrm{d}})^{\max} \simeq \frac{F^{\max}}{4\pi} \tag{6}$$

which is independent of α and β. As discussed in refs 18, 19, setting the ferromagnetic exchange coupling $J = 1$ meV as the unit of the energy, and the lattice constant $a = 5$ Å as the unit of length, the unit of the current density is $\sim 10^{13}$ A/m^2, and that of velocity is 10^3 m/sec (see Simulation Details). The typical energy density scale of a skyrmion is $E_1 \simeq D^2/J$ with D being the DM interaction. In this unit, $F_{\max}$ is also $\sim E_1$ and hence the maximum velocity $(v_x^{\mathrm{d}})^{\max}$ is roughly estimated as $\sim 10^3 \times (D/J)^2$ m/sec at the current density of $j \sim 10^{13} \times (D/J)^2\alpha$ A/m^2.

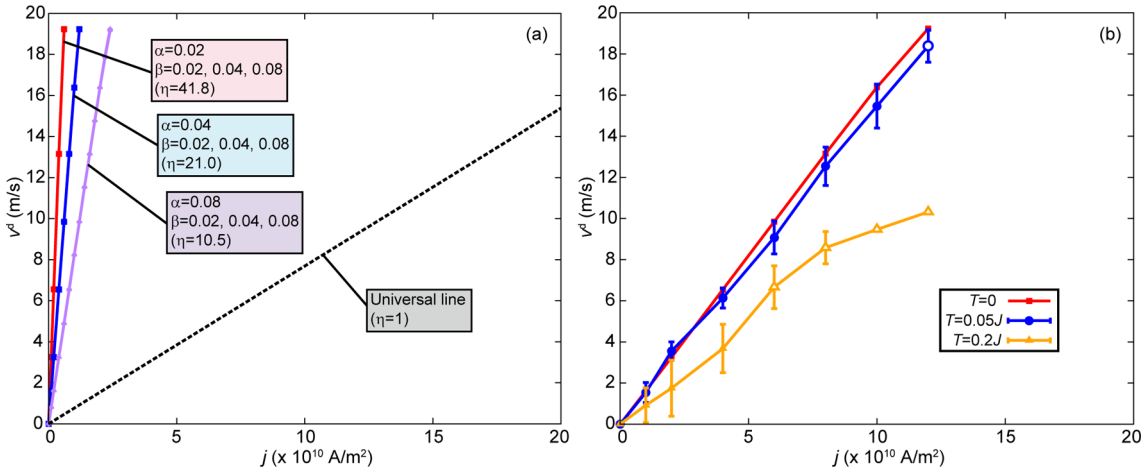

Figure 2. Steady state velocity of the current-induced motion of a skyrmion. (a) Relation between the current density j and the velocity v_x^{d} of the skyrmion for different α and β at $T = 0$. The slope η is determined only by α and does not depend on β in agreement with eq 3. Beyond the termination points, the skyrmion is annihilated at the edge. Note that the maximum velocity is independent of α and β in agreement with eq 6. The dashed line indicates the j−v^{d} relation for the skyrmion motion in a free space. (b) Relation between the current density j and the velocity v_x^{d} of the skyrmion for $(\alpha, \beta) = (0.04, 0.04)$ at several temperature. Simulations are performed four times for each j from $t = 0$ to $t = 1.3 \times 10^{-6}$ s for $j = 1.0 \times 10^{10}$ A/m^2, to $t = 6.5 \times 10^{-7}$ s for $j = 2.0 \times 10^{10}$ A/m^2, to $t = 3.9 \times 10^{-7}$ s for $j \geq 4.0 \times 10^{10}$ A/m^2. Open dot and open triangles mean that skyrmion disappeared from the edge at least once in four simulations.

dx.doi.org/10.1021/nl501379k | Nano Lett. 2014, 14, 4432−4437

This should be compared with the case of domain wall motion or the skyrmion motion in a free space, where $v^{\mathrm{d}} \sim (j/(10^{10}\ \mathrm{A/m^2}))$ m/sec. We can also discuss the effect of pinning force F_x^{pin} by adding it on the left-hand side of the first line of eq 2. One can see that the threshold v_y^{s} is given by $(v_y^{\mathrm{s}})^{\mathrm{threshold}} = F_x^{\mathrm{pin}}/(4\pi)$, which is similar to that for the skyrmion motion in free space, that is, the advantage of the extremely small threshold current density remains intact even with the constricted geometry in sharp contrast to the case of the current along the interface.[19]

Next, we confirm the predictions above by solving numerically the LLG equation under the perpendicular current. The details of the numerical simulation are provided in Simulation Details and already reported in refs 18 and 19. For the representative examples of the real-time dynamics, see Supporting Information Supplementary Movies 1 and 2. In Figure 2a, the j–v_x^{d} characteristics for different values of α and β are shown. As a reference, we plot the j–v^{d} characteristics of a skyrmion in free space (black dashed) corresponding to the slope $\eta = 1$. It is clearly seen at a glance that the slope η is much larger than unity in the present setup. The slope η is independent of β and inversely proportional to α as predicted in eq 3. The j–v^{d} relation is terminated by the disappearance of the skyrmion at certain current densities proportional to α with the common maximum value of the velocities independent of α and β, which is in good agreement with eqs 5 and 6. Beyond the prediction by the Thiele equation, we investigated the effect of finite temperature as shown in Figure 2b. At the low temperature $T = 0.05J$, the j–v^{d} characteristic shows only slight deviation from the line at $T = 0$. At the higher temperature $T = 0.2J$, however, the average velocities decrease and the skyrmion sometimes disappears from the edge even below j^{cr} because the strong thermal noise weakens the confining potential. We also performed the simulation with impurities of the strength and concentration same as in refs18 and 19, which revealed the threshold current density to drive the motion is $\sim 10^{10}$ A/m^2. This value is similar to that of the free skyrmion and much less than those of the helical phase and confined skyrmion with parallel current reported in refs 18 and 19. The motions of the confined skyrmion under the impurities with parallel current and with perpendicular current are compared in Supporting Information Supplementary Movie 3.

Now we turn to the mass and inertial motion of skyrmions in the confining potential. We consider the narrow wire and employ the harmonic potential $V(\mathbf{R}) = (Y-Y_0)^2/2K$ $(K > 0)$, where Y_0 is the coordinate of the middle line of the sample. Then, eq 1 with $\mathbf{F} = (0, -(Y - Y_0)/K)$ becomes

$$\begin{cases} -\mathcal{G}(v_y^{\mathrm{s}} - \dot{Y}) + \mathcal{D}(\beta v_x^{\mathrm{s}} - \alpha \dot{X}) + F_x = 0, & \text{(a)} \\ \mathcal{G}(v_x^{\mathrm{s}} - \dot{X}) + \mathcal{D}(\beta v_y^{\mathrm{s}} - \alpha \dot{Y}) - \dfrac{Y - Y_0}{K} + F_y = 0 & \text{(b)} \end{cases} \tag{7}$$

Substituting eq 7a into eq 7b to eliminate $\dot{Y}$, one obtains

$$\frac{Y - Y_0}{K} = \mathcal{G}(v_x^{\mathrm{s}} - \dot{X}) + (\beta - \alpha)\mathcal{D}v_y^{\mathrm{s}} + \frac{\alpha\mathcal{D}}{\mathcal{G}}F_x + F_y \tag{7c}$$

(approximations such as $(1 + (\alpha\mathcal{D}/\mathcal{G})^2) \simeq 1$ are used). Differentiating eq 7c with respect to time and substituting it into eq 7a lead

$$K\mathcal{G}^2\ddot{X} + \alpha\mathcal{D}\dot{X} + \mathcal{G}v_y^{\mathrm{s}} - \beta\mathcal{D}v_x^{\mathrm{s}} - K[\mathcal{G}^2\dot{v}_x^{\mathrm{s}} + (\beta - \alpha)\mathcal{D}\mathcal{G}\dot{v}_y^{\mathrm{s}}] = F_x + K[\alpha\mathcal{D}\dot{F}_x + \mathcal{G}\dot{F}_y] \tag{8}$$

Thus, the mass $m = K\mathcal{G}^2$ is determined by the stiffness of the confining potential.

The mass obtained above appears when the motion is driven not only by the current but also by any driving force $\mathbf{F}$. This is analogous to that of ferromagnetic domain walls.[21−23] In the case of domain walls, the wall position $\tilde{X}$ and the angle ϕ between the wall magnetization and the easy plane are canonical conjugate.[24] Magnetization anisotropy gives the potential $V(\phi)$. The equation of motion is a set of two equations including $\tilde{X}$ and ϕ, and elimination of the angle ϕ results in the equation of motion only in terms of $\tilde{X}$, where mass term appears. Similarly, in our case of skyrmions, the coordinates X and Y are canonical conjugate and the potential $V(Y)$ exists under confinement. Therefore, we have the one-to-one correspondence between two cases: $(\tilde{X}, \phi)$ to (X,Y).

To embody the statement above, we conduct the micromagnetic simulations. Here, we apply an AC current in y direction ($\mathbf{v}^{\mathrm{s}} = (0, v_0^{\mathrm{s}} \sin \omega t)$) without any other driving force ($\mathbf{F} = \mathbf{0}$). Then, eq 8 in this case is

$$K\mathcal{G}^2\ddot{X} = -\mathcal{G}v_0^{\mathrm{s}}\sin \omega t - \alpha\mathcal{D}\dot{X} + K(\beta - \alpha)\mathcal{D}\mathcal{G}\omega v_0^{\mathrm{s}}\cos \omega t \tag{9}$$

Shown in Figure 3 are the velocities $\dot{X}$ of the driven skyrmion with various parameter sets. We put the current v_y^{s} as a reference with the red line. The real-time dynamics is provided in Supporting Information Supplementary Movie 4. One can obviously see the phase shift δ of $\dot{X}$ from v_y^{s} for all the plot. When a large phase shift appears, $\ddot{X}$-term and $\dot{X}$-term are of the same order, i.e., $K\mathcal{G}^2\omega^2 \sim \mathcal{D}\alpha\omega$. Thus, we can ignore the third term in the right-hand side of eq 9 because $K(\beta - \alpha)\mathcal{D}\mathcal{G}\omega \sim (\mathcal{D}\alpha/\mathcal{G})^2 \times \mathcal{G} \ll \mathcal{G}$. Under this condition, the phase shift δ defined as $\dot{X} \propto \sin(\omega t - \delta)$ can be

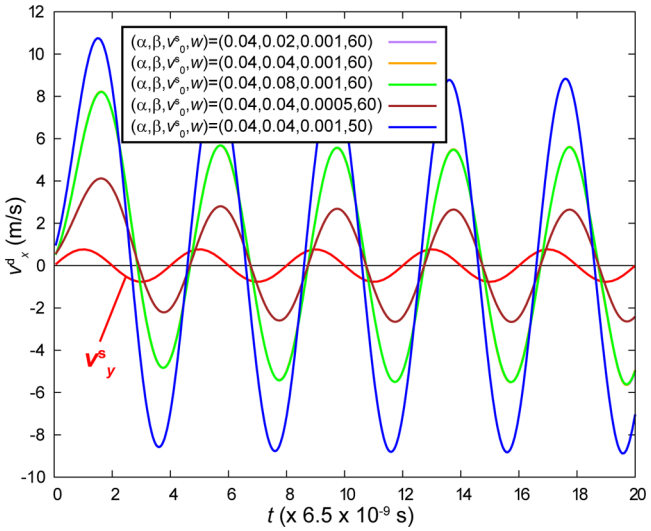

Figure 3. Calculated velocities of the skyrmion under an AC current. The red line is the applied AC current in y direction. All the velocity shows large phase shifts. Note that the purple, orange, and green curves are overlapped.

dx.doi.org/10.1021/nl501379k | Nano Lett. 2014, 14, 4432−4437

expressed as $\delta = \mathrm{Arctan}(K\mathcal{G}^2\omega/\alpha\mathcal{D})$, which is independent of β and v_0^s and in agreement with the simulated data. On the other hand, the decrease of w makes the boundary potential steep, that is, K becomes smaller, which results in the smaller phase shift δ. The estimated mass from Figure 3 is $m = K\mathcal{G}^2 = 2.56 \times 10^{-24}$ kg for the width $w = 60a$ and $m = 1.46 \times 10^{-24}$ kg for $w = 50a$. Note that there is another skyrmion mass m_{internal}, which comes from its internal deformation. This mass depends on how it is accelerated, and does not appear in the case of current-driven motion.[25] In the case of Brownian motion, the internal deformation is induced and the mass is of the order of 10^{-25} kg for the skyrmion of the same size,[25] which is an order of magnitude smaller than the mass induced by the confinement. Because the internal deformation is proportional to the number N of the spins comprising a skyrmion, the mass due to the internal deformation m_{internal} is also proportional to N. More explicitly, an estimate for this mass is $m_{\mathrm{internal}} \sim (\hbar/Ja^2)N$ since $(\hbar/Ja^2)$ is the natural unit of the mass.

Using the large mass due to the confining potential, one can emit a skyrmion from the region with transverse current to that without any current. Therefore, an experiment of the collision between the emitted skyrmion and a skyrmion at rest without the external driving current is possible.

Figure 4 displays the simulated scattering process between two skyrmions (see also Supporting Information Supplementary Movie 5). First, the motion of one skyrmion (skyrmion 1) is driven by a DC current in y direction in the region of $i_x < 300$ ((i_x,i_y) is a site index), whereas the other skyrmion (skyrmion 2) is at rest (Figure 4a). Note that the y coordinate Y_1 of the skyrmion 1 is above the central line Y_0 of the channel. Here, y coordinate Y can be regarded as the kinetic momentum of the skyrmion since we get $-\mathcal{G}(Y - Y_0) = m\dot{X}$ from eq 7b neglecting the small damping term. Driven skyrmion 1 enters into the region without current (Figure 4b). Although there is no driving force in this region, inertia keeps the velocity of skyrmion 1. In Figure 4c and d, the scattering between skyrmions 1 and 2 occurs. After their collision, skyrmion 1 stops, and skyrmion 2 has a finite velocity in x direction with its y coordinate Y_2 getting larger than Y_0 (Figure 4e).

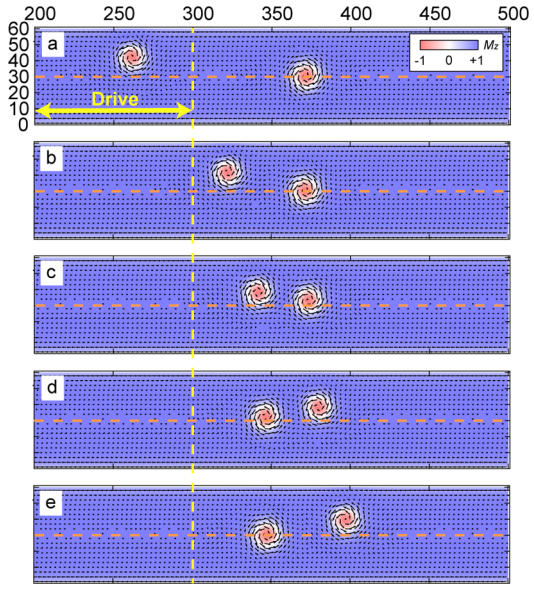

Figure 4. Scattering process between two skyrmions at selected times. In-plane components of the magnetic moments at sites (i_x,i_y) are shown by arrows when $\mathrm{mod}(i_x,3) = \mathrm{mod}(i_y,3) = 1$. The color represents the out-of-plane components of the magnetic moments. The orange dashed line is the central line of the wire. A DC current of y direction is applied in the region $i_x < 300$ (left to the yellow dashed line). (a) $t = 1.46 \times 10^{-8}$ s. (b) $t = 1.69 \times 10^{-8}$ s. (c) $t = 1.79 \times 10^{-8}$ s. (d) $t = 1.85 \times 10^{-8}$ s. (e) $t = 1.95 \times 10^{-8}$ s.

The time evolution of the coordinates X_1, Y_1, X_2 and Y_2 of two skyrmions is depicted in Figure 5a. The coordinate X_1 grows proportional to t^2 for small t and linearly for large t. This feature is characterized by the finite mass, and we confirmed that the value of the mass obtained above in the AC current response is quantitatively consistent with this curve. When they interact, the quantity $Y_1 + Y_2$, which acts as total momentum, is conserved although the small decay of it is observed due to the damping effect. The y coordinate Y_2 of the skyrmion 2 starts to increase when the distance $X_2 - X_1$ between the skyrmions 1 and 2 is about the size ξ of the skyrmion; there is a short-range interaction between skyrmions. After their interaction, Y_1 remains to be Y_0; we can conclude that the scattering is almost elastic. Because skyrmion consists of many spins, there should be a large number of internal excitations. However, the scattering time Δt is $\Delta t \sim 2.3 \times 10^{-9}$ s, and the corresponding energy scale E of the scattering is $E \sim \hbar/\Delta t \sim 2.86 \times 10^{-4}$ meV, which is much smaller than the magnon gap $B = 2.78 \times 10^{-2}$ meV (see Simulation Details for the parameters in our numerical simulations). Therefore, the contribution of internal modes is negligible, that is, there is almost no internal deformation of the skyrmions as seen in Figure 4. Even at finite temperature $T = 0.05J$, the motion is just separated into the elastic scattering and the Brownian motion (Figure 5b). Note that the temperature $T = 0.05J$ is larger than the gap in the magnon spectrum, and thermally excited magnons cause only the Brownian motion and do not affect the elastic scattering. This finding of the elastic short-range scattering between skyrmions will be useful for the design of the logic gates using skyrmions.

In conclusion, we have studied the skyrmion dynamics near the edge driven by the transverse current, which has the several advantages over that by the parallel current. The j–v^{d} characteristic shows a steep slope ($\sim 1/\alpha$) with the small threshold current density. The skyrmion obtains the mass due to the confining potential, which gives the inertial motion after the current is switched off, which enables the "skyrmion gun". Using this property, we did the numerical simulation of the collision process between the two skyrmions, which clearly indicates that the interaction between them is repulsive and short-range and almost elastic scattering occurs. The exchange of the coordinate transverse to the edge clearly shows that it plays the role of kinetic momentum and is conserved. These findings will form the basis for the design of skyrmion devices in confined geometries.

Simulation Details. We consider the lattice model of chiral magnets with the following Hamiltonian H

$$H = -J\sum_{\mathbf{r}} \mathbf{M}_{\mathbf{r}}\cdot(\mathbf{M}_{\mathbf{r}+a\mathbf{e}_x} + \mathbf{M}_{\mathbf{r}+a\mathbf{e}_y}) - D\sum_{\mathbf{r}} (\mathbf{M}_{\mathbf{r}} \times \mathbf{M}_{\mathbf{r}+a\mathbf{e}_x}\cdot\mathbf{e}_x + \mathbf{M}_{\mathbf{r}} \times \mathbf{M}_{\mathbf{r}+a\mathbf{e}_y}\cdot\mathbf{e}_y) - \mathbf{B}\cdot\sum_{\mathbf{r}} \mathbf{M}_{\mathbf{r}} - A\sum_{\mathbf{r}\in I} (M_{\mathbf{r}z})^2 \quad (10)$$

dx.doi.org/10.1021/nl501379k | Nano Lett. 2014, 14, 4432–4437

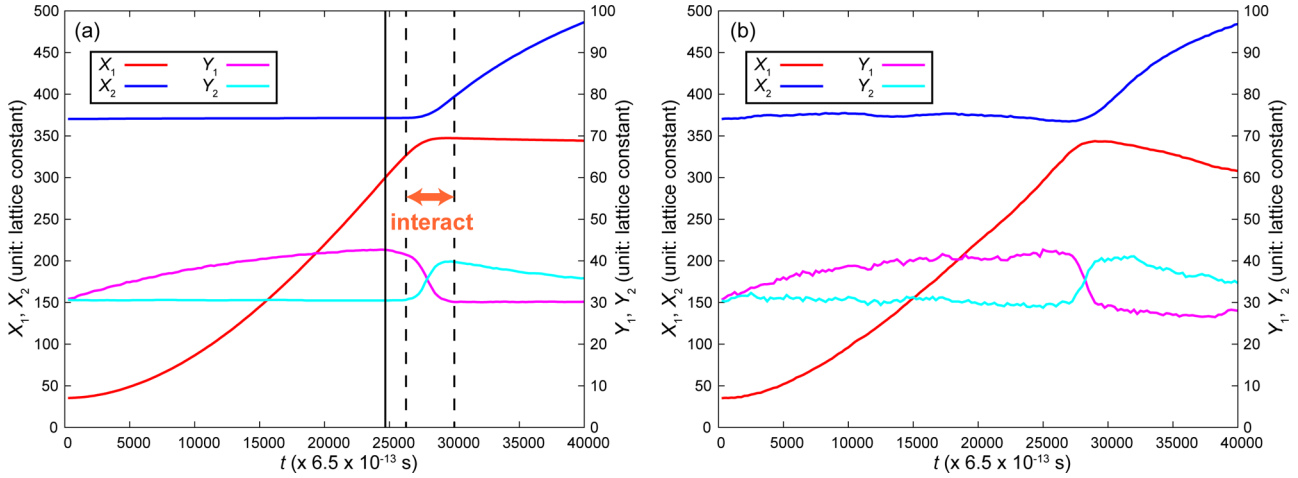

Figure 5. Time evolution of the coordinates X_1, Y_1, X_2, and Y_2 of two skyrmions. Note that the axis for X_1 and X_2 and that for Y_1 and Y_2 are different. (a) At $T = 0$. Skyrmion 1 enters the region without any current at $t = 1.66 \times 10^{-8}$ s (black solid line). Skyrmions 1 and 2 interact with each other between $t = 1.72 \times 10^{-8}$ s and $t = 1.95 \times 10^{-8}$ s (black dashed lines). (b) At $T = 0.05J$.

where $\mathbf{M}_\mathbf{r}$ is the magnetization direction at $\mathbf{r}$ treated as a classical dimensionless vector, a is a lattice constant, and $\mathbf{e}_i$ is the unit vector to i direction. The forth term is introduced as the effect of pinning centers controlled by the strength A and the distribution I. Our numerical simulations are based on the LLG equation

$$\frac{d\mathbf{M}_\mathbf{r}}{dt} = -\mathbf{M}_\mathbf{r} \times [\mathbf{B}_\mathbf{r}^{\mathrm{eff}} + \mathbf{B}_\mathbf{r}^{\mathrm{th}}(t)] + \frac{\alpha}{M}\mathbf{M}_\mathbf{r} \times \frac{d\mathbf{M}_\mathbf{r}}{dt} + \mathbf{T}^{\mathrm{STT}} \tag{11}$$

$$\mathbf{T}^{\mathrm{STT}} \equiv -(\mathbf{v}^s \cdot \nabla)\mathbf{M}_\mathbf{r} + \frac{\beta}{M}[\mathbf{M}_\mathbf{r} \times (\mathbf{v}^s \cdot \nabla)\mathbf{M}_\mathbf{r}] \tag{12}$$

with $\mathbf{B}_\mathbf{r}^{\mathrm{eff}} \equiv -(1/\hbar)(\partial H/\partial \mathbf{M}_\mathbf{r})$. The stochastic field $\mathbf{B}_\mathbf{r}^{\mathrm{th}}(t)$ describes the thermal noise, which has the following properties: $\langle B_{\mathbf{r}i}^{\mathrm{th}}(t)\rangle = 0, \langle B_{\mathbf{r}i}^{\mathrm{th}}(t) B_{\mathbf{r}'i}^{\mathrm{th}}(s)\rangle = (\alpha k_\mathrm{B} T/M)\delta_{\mathbf{r}\mathbf{r}'}\delta_{ij}\delta(t-s)$.

The parameters J, D, and B are chosen to be realistic values $J = 1$ meV, $D = 0.18J$, and $B = 0.0278J$ same as in refs 18 and 19. To solve the LLG equation, we use the fourth-order Runge–Kutta method for $T = 0$ and the Heun method[26,27] for $T > 0$. The periodic boundary condition is imposed for the x direction, whereas the open boundary condition is used for y direction. The units of time t, current density j, velocity v^d, and mass m with a typical lattice constant $a = 5$ Å, spin-polarization $p = 0.2$, and the magnitude of local magnetic moment M = 1 are $\hbar/J \simeq 6.5 \times 10^{-13}$ s, $(2eMJ/pa^2\hbar) \simeq 1.0 \times 10^{13}$ A/m^2, $(aJ/\hbar) \simeq 7.7 \times 10^{12}$ m/sec, and $(\hbar^2/Ja^2) \simeq 2.8 \times 10^{-28}$ kg, respectively. We use these values to convert the units of simulated current density and time.

■ ASSOCIATED CONTENT

Supporting Information

Supplementary Movie 1: Skyrmion motion near the interface extending along x direction between the chiral magnet with DM interaction and the lead. The current is flowing perpendicular to the interface (y direction). In-plane components of the magnetic moments at sites (i_x,i_y) are represented by arrows when $\mathrm{mod}(i_x,3) = \mathrm{mod}(i_y,3) = 1$ in a system of 100×120 sites for a time range from $t = 0$ to $t = 5.2 \times 10^{-8}$ s. The numerical simulation is performed for $(\alpha, \beta) = (0.04,0.04)$ with current density $j = 1.0 \times 10^{10}$ A/m^2. We take the periodic boundary condition along x direction. The DM interaction D is set to be 0.18 in the unit of ferromagnetic exchange interaction $J = 1$. This determines the diameter of the skyrmion as ∼35 lattice sites. Supplementary Movie 2: Skyrmion motion in a nanowire driven by DC current perpendicular to it. In-plane components of the magnetic moments at sites (i_x,i_y) are represented by arrows when $\mathrm{mod}(i_x,3) = \mathrm{mod}(i_y,3) = 1$ in a system of 300×60 sites for a time range from $t = 0$ to $t = 6.5 \times 10^{-8}$ s. The numerical simulation is performed for $(\alpha,\beta) = (0.04,0.04)$ with current density along y direction $j = 1.0 \times 10^{10}$ A/m^2. Supplementary Movie 3: Comparison of a skyrmion motions in a nanowire driven by DC current parallel and perpendicular to the edge. The top two panels show the motion with current in x direction, and the bottom two in y direction. The magnetization direction is represented by color in a system of 600×50 sites for a time range from $t = 0$ to $t = 9.7 \times 10^{-8}$ s. The numerical simulations are performed for $(\alpha,\beta) = (0.04,0.04)$ and $(0.04,0)$ with current density $j = 1.0 \times 10^{10}$ A/m^2. Supplementary Movie 4: Skyrmion motion in a nanowire driven by AC current perpendicular to it. In-plane components of the magnetic moments at sites (i_x,i_y) are represented by arrows when $\mathrm{mod}(i_x,3) = \mathrm{mod}(i_y,3) = 1$ in a system of 300×60 sites for a time range from $t = 0$ to $t = 1.3 \times 10^{-7}$ s. The numerical simulation is performed for $(\alpha,\beta) = (0.04,0.04)$ with current density along y direction $j = 1.0 \times 10^{10}$ A/m^2 $\times$ sin ωt with the frequency $\omega = 6.1 \times 10^7$ s^{-1}. The inset shows the velocity of the skyrmion (red) and the current (blue). Supplementary Movie 5: Collision of two skyrmions in a nanowire. In-plane components of the magnetic moments at sites (i_x,i_y) are represented by arrows when $\mathrm{mod}(i_x,3) = \mathrm{mod}(i_y,3) = 1$ in a system of 500×60 sites for a time range from $t = 0$ to $t = 2.5 \times 10^{-8}$ s. The numerical simulation is performed for $(\alpha,\beta) = (0.04,0.04)$ with current density along y direction $j = 1.0 \times 10^{10}$ A/m^2 in the region of $i_x < 300$. This material is available free of charge via the Internet at http://pubs.acs.org.

■ AUTHOR INFORMATION

Corresponding Author

*E-mail: iwasaki@appi.t.u-tokyo.ac.jp.

Notes

The authors declare no competing financial interest.

■ ACKNOWLEDGMENTS

This work was supported by Grant-in-Aids for Scientific Research (No. 24224009 and No. 24360036) from the Ministry of Education, Culture, Sports, Science and Technology (MEXT) of Japan, and Strategic International Cooperative Program (Joint Research Type) from Japan Science and Technology Agency. J.I. was supported by Grant-in-Aids for JSPS Fellows (No. 2610547).

■ REFERENCES

(1) Skyrme, T. H. R. *Nucl. Phys.* **1962**, *31*, 556.
(2) Bogdanov, A. N.; Yablonskii, D. A. *Sov. Phys.—JETP* **1989**, *68*, 101.
(3) Rössler, U. K.; Bogdanov, A. N.; Pfleiderer, C. *Nature* **2006**, *442*, 797.
(4) Mühlbauer, S.; Binz, B.; Jonietz, F.; Pfleiderer, C.; Rosch, A.; Neubauer, A.; Georgii, R.; Böni, P. *Science* **2009**, *323*, 915.
(5) Yu, X. Z.; Onose, Y.; Kanazawa, N.; Park, J. H.; Han, J. H.; Matsui, Y.; Nagaosa, N.; Tokura, Y. *Nature* **2010**, *465*, 901.
(6) Yu, X. Z.; Kanazawa, N.; Onose, Y.; Kimoto, K.; Zhang, W. Z.; Ishiwata, S.; Matsui, Y.; Tokura, Y. *Nat. Mater.* **2011**, *10*, 106.
(7) Heinze, S.; von Bergmann, K.; Menzel, M.; Brede, J.; Kubetzka, A.; Wiesendanger, R.; Bihlmayer, G.; Blügel, S. *Nat. Phys.* **2011**, *7*, 713.
(8) Seki, S.; Yu, X. Z.; Ishiwata, S.; Tokura, Y. *Science* **2012**, *336*, 198.
(9) Nagaosa, N.; Tokura, Y. *Nat. Nanotechnol.* **2013**, *8*, 899.
(10) Jonietz, F.; Mühlbauer, S.; Pfleiderer, C.; Neubauer, A.; Münzer, W.; Bauer, A.; Adams, T.; Georgii, R.; Böni, P.; Duine, R. A.; Everschor, K.; Garst, M.; Rosch, A. *Science* **2010**, *330*, 1648.
(11) Schulz, T.; Ritz, R.; Bauer, A.; Halder, M.; Wagner, M.; Franz, C.; Pfleiderer, C.; Everschor, K.; Garst, M.; Rosch, A. *Nat. Phys.* **2012**, *8*, 301.
(12) Yu, X. Z.; Kanazawa, N.; Zhang, W. Z.; Nagai, T.; Hara, T.; Kimoto, K.; Matsui, Y.; Onose, Y.; Tokura, Y. *Nat. Commun.* **2012**, *3*, 988.
(13) Ono, T. Spin-transfer torque in nonuniform magnetic structures. In *Spin Current*; Maekawa, S., Valenzuela, S. O., Saitoh, E., Kimura, T., Eds.; Oxford University Press: New York, 2012; pp 402−423.
(14) Maekawa, S. *Concepts in Spin Electronics*; Oxford University Press: Oxford, 2006; Ch. 7.
(15) Parkin, S. S. P.; Hayashi, M.; Thomas, L. *Science* **2008**, *320*, 190−194.
(16) Thiele, A. A. *Phys. Rev. Lett.* **1973**, *30*, 230.
(17) Everschor, K.; Garst, M.; Binz, B.; Jonietz, F.; Mühlbauer, S.; Pfleiderer, C.; Rosch, A. *Phys. Rev. B: Condens. Matter Mater. Phys.* **2012**, *86*, 054432.
(18) Iwasaki, J.; Mochizuki, M.; Nagaosa, N. *Nat. Commun.* **2013**, *4*, 1463.
(19) Iwasaki, J.; Mochizuki, M.; Nagaosa, N. *Nat. Nanotechnol.* **2013**, *8*, 742.
(20) Sampaio, J.; Cros, V.; Rohart, S.; Thiaville, A.; Fert, A. *Nat. Nanotechnol.* **2013**, *8*, 839.
(21) Saitoh, E.; Miyajima, H.; Yamaoka, T.; Tatara, G. *Nature* **2004**, *432*, 203.
(22) Clarke, D. J.; Tretiakov, O. A.; Chern, G.-W.; Bazaliy, Ya. B.; Tchernyshyov, O. *Phys. Rev. B: Condens. Matter Mater. Phys.* **2008**, *78*, 134412.
(23) Zvezdin, A. K.; Zvezdin, K. A. *Low Temp. Phys.* **2010**, *36*, 826.
(24) Takagi, S.; Tatara, G. *Phys. Rev. B: Condens. Matter Mater. Phys.* **1996**, *54*, 9920.
(25) Unpublished data by Schütte, C.; et al..
(26) García-Palacios, J. L.; Lázaro, F. J. *Phys. Rev. B: Condens. Matter Mater. Phys.* **1998**, *58*, 14937.
(27) We use a random-number generator developed by M. Matsumoto and T. Nishimura. http://www.math.sci.hiroshima-u.ac.jp/~m-mat/MT/emt.html (accessed May 2014).